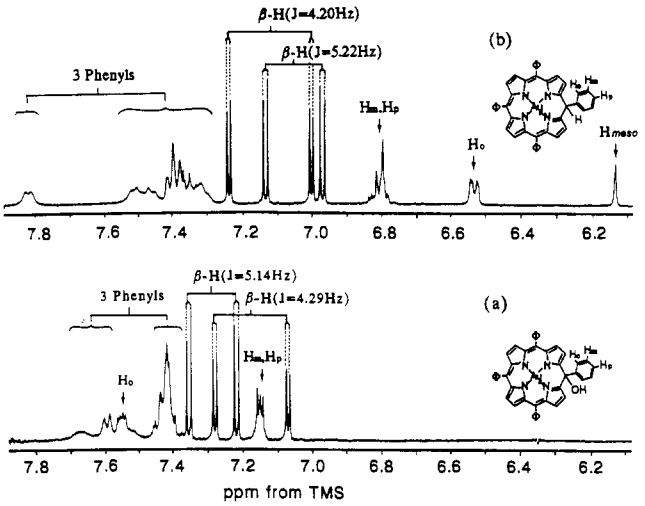

Figure 3. The 400-MHz ^{1}H NMR spectra of (a) [Au^{III}(TPP-OH)] (**1**) and (b) [Au^{III}(TPP-H)] (**2**) in cyclohexane-d_{12}.

The nucleophilic addition of OH^- to gold(III) tetraphenylporphine chloride[11] ([Au^{III}(TPP)]$^+$Cl$^-$) was performed by the following procedure. A slight excess of aqueous NaOH was added to a DMSO solution of [Au^{III}(TPP)]$^+$Cl$^-$ at room temperature. As NaOH was added, the solution color changed form red to greenish brown. This reaction proceeded in other solvents such as DMF and with other OH^- ion sources such as TBAOH. The greenish brown product **1** (Chart I) was isolated by extraction with *n*-hexane. The *n*-hexane solution was washed twice with water to remove ionic species and evaporated to remove the solvent, and then the product **1** was dried in vacuo at room temperature. The absorption spectrum of **1** (Figure 2) differs clearly from that of π-radical species, metal redox species, ligand exchange species, and isoporphyrins.[7,9] It is noteworthy that the absorption spectrum of **1** resembles that of gold(III) tetraphenylphlorin **2** in the features of the visible and the near-infrared absorption bands (Figure 2) except for the blue shifts of the absorption maxima.[12] These results suggest that the π-electron system of the porphyrin ring of **1** is broken as is that of **2**. The following data were obtained for the molecular structure of **1**. (i) The molecular weight (MW) of **1** determined by secondary ion mass spectrometry (SIMS) was 826, indicating that **1** was a monohydroxylated product of [Au^{III}(TPP)]$^+$ (MW = 809).[13] (ii) The MH$^+$ SIMS peak indicates that the product is a neutral species.[13] (iii) Bands at 3572 and 3607 cm^{-1} in the infrared absorption spectrum of **1** in CCl_4 revealed that the OH group was attached as an alcoholic OH (supplementary material). (iv) Although [Au^{III}(TPP)]$^+$Cl$^-$ exhibits weak infrared absorption in the range 1400–1700 cm^{-1}, **1** has very strong bands in this region as does **2** (supplementary material). These bands arise from the activation of a porphyrin vibration by the breaking of D_{4h} symmetry.[14] (v) As shown in Figure 3, the ^{1}H NMR spectrum for the β-protons of **1** consists of two AB quartets, which indicates that **1** has C_2 symmetry due to addition at one meso carbon.[15] Consequently, it was concluded that **1** is gold (III) tetraphenylporphyrin monohydroxylated at the meso position, namely, "hydroxyphlorin" (Au^{III}(TPP-OH)).[16] The OH group of **1** was reversibly eliminated by the addition of acid, but the phenyl group was not eliminated. We could understand **1** as Meisenheimer complex analogous to the nucleophilic adduct derived from trinitrobenzene and hydroxide anion.

The optical spectra of isoporphyrins containing a divalent or trivalent central metal are quite different from the spectra of **1** and **2**.[7] The isoporphyrins have two strong absorption peaks in the near-IR region, but the phlorins have only one broad peak in the near-IR region. Therefore the isoporphyrin and the phlorin can be easily differentiated by the absorption spectra.

For other gold(III) porphyrins ([Au^{III}(TPyP)]$^+$Cl$^-$, [Au^{III}(TSPP)]$^+$Cl$^-$, and [Au^{III}(TCPP)]$^+$Cl$^-$), the corresponding nucleophilic adducts were obtained by the same procedure.[17] On the other hand, nucleophilic adducts of Pd^{II}(TPP), Cu^{II}(TPP), Cd^{II}(TPP), and [Mn^{III}(TPP)]$^+$Cl$^-$ were not formed even in the DMSO solution saturated with TBAOH. These results are interpreted in terms of differences in the electrophilicity of the porphyrin ring, which are induced by the central metal. From these results, we expect that similar nucleophilic addition occurs in other porphyrins with high-valence metals such as P(V). The present reaction is regarded as not only an important feature of porphyrins with high-valence metals but also a novel route for the modification of porphyrins.

Acknowledgment. We thank Prof. Tamio Ueno and Dr. Chul-Sa Kim of Kyoto University for the SIMS measurements. This work was partially supported by grants from the Ministry of Education, Science, and Culture of the Japanese Government. This work was also funded by the Photo Science and Technology Foundation.

Supplementary Material Available: Infrared absorption spectra of **1**, **2**, and [Au^{III}(TPP)]$^+$Cl$^-$ (1 page). Ordering information is given on any current masthead page.

(11) Anal. Calcd for [Au^{III}(TPP)]$^+$Cl$^-$·2H$_2$O, $C_{44}H_{32}N_4O_2AuCl$: C, 60.0; H, 3.54; N, 6.49; Cl, 4.04. Found: C, 60.5; H, 3.43; N, 6.35; Cl, 4.02.

(12) The absorption maxima of **1** in C_6H_{12} are 439 nm ($\epsilon = 6.9 \times 10^4$) and 726 nm ($\epsilon = 1.9 \times 10^4$). The absorption maxima of **2** in C_6H_{12} are 443 nm ($\epsilon = 5.8 \times 10^4$) and 756 nm ($\epsilon = 1.6 \times 10^4$). The phlorin **2** was obtained by the chemical reduction of [Au^{III}(TPP)]$^+$ according to ref 8.

(13) A Hitachi M80 was used for the secondary ion mass spectrometry. Obtained parent peaks are 827 (MH$^+$) for **1**, 811 (MH$^+$) for **2**, and 809 (M$^+$) for [Au^{III}(TPP)]$^+$.

(14) Bürger, H. *Porphyrins and Metalloporphyrins*; Smith, K. M., Ed.; Elsevier: Amsterdam, 1975; Chapter 11.

(15) The two AB quartets in the ^{1}H NMR spectra of the β-protons were observed in both phlorin[4] and isoporphyrin.[5] The ^{1}H NMR spectral data of the β-protons of **1** are as follows: 7.07 (d, 2 H, J_{HH} = 4.29 Hz), 7.22 (d, 2 H, J_{HH} = 5.14 Hz), 7.28 (d, 2 H, J_{HH} = 4.29 Hz), 7.35 ppm (d, 2 H, J_{HH} = 5.14 Hz). Those of **2** are as follows: 6.97 (d, 2 H, J_{HH} = 5.22 Hz), 7.00 (d, 2 H, J_{HH} = 4.20 Hz), 7.14 (d, 2 H, J_{HH} = 5.22 Hz), 7.24 ppm (d, 2 H, J_{HH} = 4.20 Hz). The chemical shifts of **1** are at lower field than those of **2** because of the presence of an O atom in **1**.

(16) An IUPAC name for **1** is inconvenient for the distinction from the corresponding isoporphyrin. As a trivial name, the term "hydroxyphlorin" could be conveniently used for the designation of **1** in order to distinguish it from the normal phlorins and isoporphyrins.

(17) Absorption maxima of hydroxyphlorins in DMSO are as follows: 438 and 719 nm for [Au^{III}(TPyP-OH)], 441 and 725 nm for [Au^{III}(TSPP-OH)], and 441 and 727 nm for [Au^{III}(TCPP-OH)].

Role of F Centers in the Oxidative Coupling of Methane to Ethane over Li-Promoted MgO Catalysts

Ming-Cheng Wu, Charles M. Truong, Kent Coulter, and D. Wayne Goodman*

Department of Chemistry, Texas A&M University College Station, Texas 77843-3255

Received April 6, 1992

We report a study of the partial oxidation of methane to ethane over a model MgO catalyst prepared under well-controlled, ultrahigh vacuum (UHV) conditions using a combination of surface science techniques and elevated pressure kinetic measurements. The results indicate that [Li$^+$O$^-$] centers are not likely to be directly involved in the methane activation step, but rather they promote the production of color centers in the near-surface region which are responsible for this key step in the methane coupling reaction.

Li-promoted MgO films were synthesized under UHV conditions by co-depositing Mg and Li onto a clean Mo(100) surface in a background pressure of oxygen. A detailed description regarding film synthesis and characterization will be given elsewhere.[1] The oxide films were pretreated by heating in oxygen

* Author to whom correspondence should be addressed.

0002-7863/92/1514-7565$03.00/0

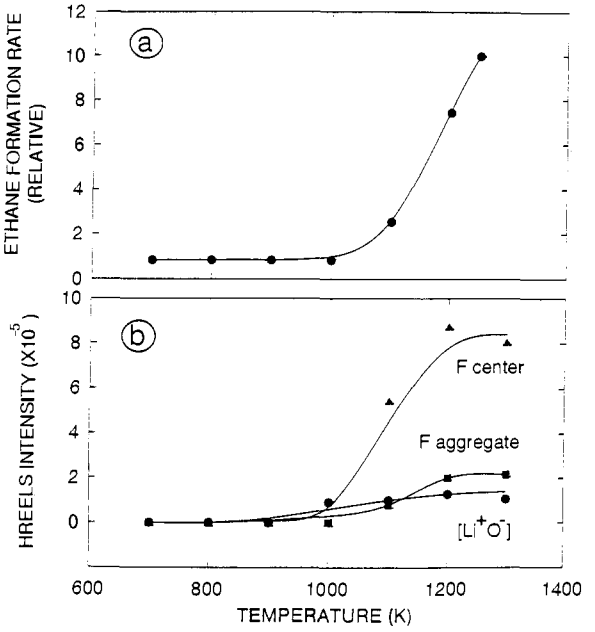

Figure 1. (a) Ethane formation rate measured at 990 K as a function of sample pretreatment temperature. The Li loading was approximately 10 at percent. (b) HREELS intensities of the various defects normalized to the respective elastic peak versus the sample pretreatment temperature. The Li content was 10 at percent.

to various temperatures (700–1300 K) prior to reaction.

The reaction was carried out at 990 K under 6 Torr of reactants with an O_2:CH_4 ratio of 1:5 in a combined elevated pressure reactor/UHV surface analysis chamber.[2] After a 5-min reaction, the product gas mixture was analyzed with gas chromatography utilizing a flame ionization detector. The ethane production at 990 K as a function of the sample pretreatment temperature exhibits a 10-fold increase as the temperature is increased from 1000 to 1250 K, as shown in Figure 1a.

Model thin films prepared in the same manner as those used in the kinetic experiments were characterized in a high-resolution electron energy loss spectroscopy (HREELS) system,[3] which was employed to investigate the electronic transitions associated with a variety of defects.[1] Figure 2 presents a set of HREELS spectra acquired as a function of sample pretreatment temperature. The spectra obtained from these films exhibit a prominent loss feature at 6.3 eV. This feature is believed to be due to a surface-related interband transition of MgO.[4,5] Upon annealing to $T \geq 1000$ K, a distinct loss feature at ~1.6 eV emerges and becomes saturated in intensity with increasing temperature. Two additional loss features are apparent at 3.6 and 5.3 eV following an anneal to ≥1100 K. Further studies including the electron beam energy dependence of these features indicate that the species giving rise to these excitations are in the near-surface region.[1] In Figure 1b, the normalized intensities of these losses are plotted as a function of the pretreatment temperature.

Abraham and co-workers[6-8] have shown that the production of the [Li$^+$O$^-$] centers gives rise to a characteristic resonance at $g_\perp = 2.054$ in electron spin resonance spectra and to a characteristic feature which is at a maximum at 1.8 eV in the optical

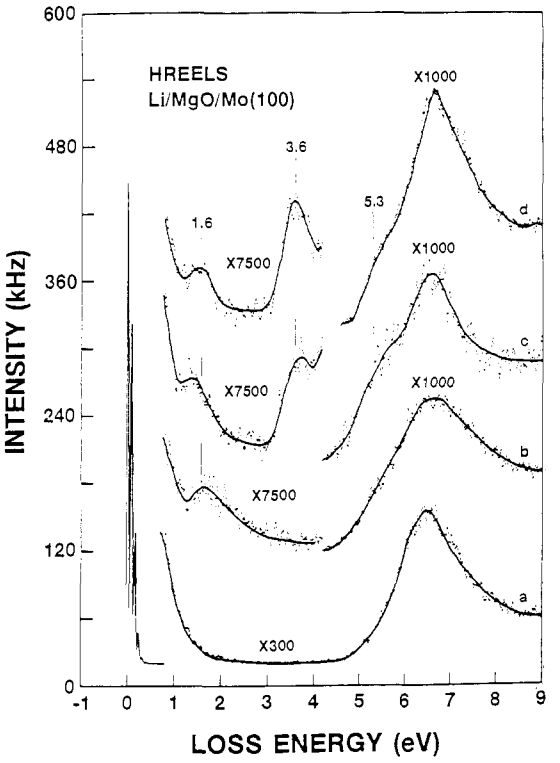

Figure 2. HREELS spectra acquired subsequent to annealing a 10 at percent Li-doped MgO film in 5×10^{-7} Torr of oxygen to various temperatures: (a) 300; (b) 1000; (c) 1200; (d) 1300 K. The film thickness is 20 monolayers. The spectral data were collected using an electron beam with primary energy of 15 eV at a sample temperature of 80 K.

absorption spectrum. The loss feature observed at ~1.6 eV therefore confirms the presence of [Li$^+$O$^-$] centers in the near-surface region in our MgO films. The 3.6 and 5.3 eV loss features are likewise assigned to correspond to F aggregates and F centers (oxygen vacancies containing two electrons) in MgO, respectively, since two identical peaks have been observed in pure MgO films and have been attributed to these defect centers.[1,9-11]

The conclusion that [Li$^+$O$^-$] centers are directly responsible for the methane activation has been derived primarily from several experiments in which the number of methyl radicals formed[12] and the rate of ethane formation[13] were found to parallel the density of [Li$^+$O$^-$] centers as the Li concentration was varied. The present studies, however, show that for a particular Li concentration (10 at percent) the [Li$^+$O$^-$] HREELS intensity remains essentially constant in the 1000–1300 K temperature region whereas a 10-fold increase is observed in the ethane yield. This behavior thus is contrary to the assumption that [Li$^+$O$^-$] centers play a direct role in the methane activation step.[14,15] On the other hand, it is found that the concentration of F centers (F aggregates) and the ethane production change in concert as shown in Figure 1, consistent with the F centers being directly responsible for the methane activation step. It follows then that the generation of methyl radicals occurs via surface F centers, namely, surface sites of low coordination. These surface sites are assumed to be in equilibrium with bulk F centers and F aggregates at the high temperatures typically used for this reaction.

Further support for our argument that F centers rather than [Li$^+$O$^-$] centers are the key reaction sites is that pure MgO

(1) Wu, M.-C.; Truong, C. M.; Goodman, D. W. *Phys. Rev. B*, in press.
(2) Coulter, K.; Goodman, D. W. *Catal. Lett.*, in press.
(3) Parmeter, J. E.; Jiang, X.; Goodman, D. W. *Surf. Sci.* **1990**, *240*, 85–100.
(4) Henrich, V. E.; Dresselhaus, G.; Zeiger, H. J. *Phys. Rev. B* **1980**, *22*, 4764–4775.
(5) Wu, M.-C.; Corneille, J. S.; Estrada, C. A.; He, J.-W.; Goodman, D. W. *Chem. Phys. Lett.* **1991**, *182*, 472–477.
(6) Abraham, M. M.; Chen, Y.; Boatner, L. A.; Reynolds, R. W. *Phys. Rev. Lett.* **1976**, *37*, 849–852.
(7) Chen, Y.; Tohver, H. T.; Narayan, J.; Abraham, M. M. *Phys. Rev. B* **1977**, *16*, 5535–5542.
(8) Olson, D. N.; Orera, V. M.; Chen, Y.; Abraham, M. M. *Phys. Rev. B* **1980**, *21*, 1258–1263.
(9) Weber, H. *Z. Phys.* **1951**, *30*, 392.
(10) Hensley, H. B.; Kroes, R. L. *Bull. Am. Phys. Soc.* **1986**, *13*, 420.
(11) Henderson, B.; Wertz, J. E. *Defects in the Alkaline Earth Oxides*; Taylor & Francis LDT: London, 1977.
(12) Driscoll, D. J.; Martir, W.; Wang, J.-X.; Lunsford, J. H. *J. Am. Chem. Soc.* **1985**, *107*, 58–63.
(13) Ito, T.; Wang, J.-X.; Lin, C.-H.; Lunsford, J.-H. *J. Am. Chem. Soc.* **1985**, *107*, 5062–5068.
(14) Ito, T.; Lunsford, J. H. *Nature (London)* **1985**, *314*, 721–722.
(15) Lunsford, J. H. *Catal. Today* **1990**, *6*, 235–259.

catalysts exhibit an apparent activation energy of ~60 kcal/mol for ethane formation.[2,12-15] This value is approximately the same as that found for Li-doped MgO,[2,12-15] although the activity of pure MgO is some 10-fold lower. The enhanced activity of Li-promoted MgO catalysts for ethane production is thus a predictable consequence of the increase in the density of F centers and F aggregates in the near-surface region which occurs following the addition of Li and MgO.

Acknowledgment. We acknowledge with pleasure the support of this work by the Gas Research Institute and the Department of Energy, Office of Basic Energy Sciences, Division of Chemical Science.

Model Complexes for α-Keto Acid-Dependent Enzymes. Structure and Reactivity of {Fe^{II}[tris[(6-methyl-2-pyridyl)methyl]amine](benzoylformate)}(ClO_4)

Yu-Min Chiou and Lawrence Que, Jr.*

Department of Chemistry, University of Minnesota
Minneapolis, Minnesota 55455

Received March 2, 1992

α-Keto acid-dependent enzymes[1] catalyze a wide variety of reactions involving the oxidative decarboxylation of a keto acid concomitant with the functionalization of an unreactive C-H bond.[2] For hydroxylases, one atom from dioxygen is introduced into the substrate (S) and the other into the resulting carboxylic acid.[3] Examples of this type of enzyme include prolyl 4-

$$S + O_2 + RCOCOOH \rightarrow SO + RCOOH + CO_2$$

hydroxylase,[4] 4-hydroxyphenylpyruvate dioxygenase,[5] and thymine hydroxylase.[6] Fe(II) appears to be required for reactivity;[7,8] however, little is known about the reaction mechanism or the coordination environment around the metal center. A plausible mechanism has been proposed in which the α-keto acid is oxidatively decarboxylated to produce a reactive intermediate, which then hydroxylates the susceptible substrate.[9] This mechanism is supported by the uncoupling of the 2-oxoglutarate decarboxylation from hydroxylation in reactions catalyzed by proline, γ-butyrobetaine, and thymine hydroxylases in the presence of substrate analogues.[10] Herein, we report the synthesis of the first Fe^{II}-α-keto acid complexes, their physical properties, and their reactivity with dioxygen.

Treatment of $Fe(ClO_4)_2 \cdot 6H_2O$ with equimolar amounts of TLA[11] or TPA[12,13] and benzoylformate (BF) in methanol affords

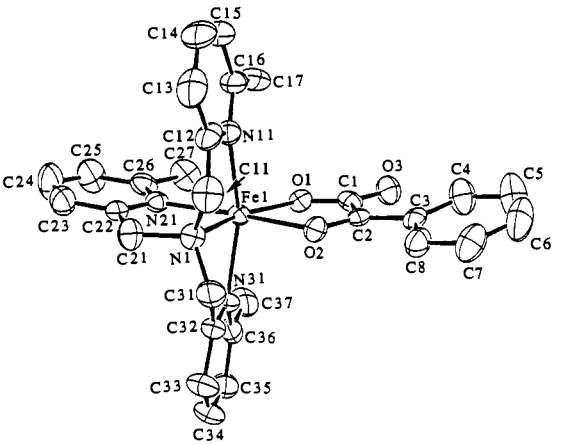

Figure 1. ORTEP view of $[Fe^{II}(TLA)(BF)]^+$, showing 50% probability thermal ellipsoids and atom labeling scheme. Hydrogen atoms are omitted for clarity. Selected bond distances (Å) and angles (deg) are as follows: Fe-O1, 2.001 (4); Fe-O2, 2.212 (4); Fe-N1, 2.171 (5); Fe-N11, 2.273 (6); Fe-N21, 2.166 (5); Fe-N31, 2.231 (6); O1-Fe-O2, 75.3 (2); O1-Fe-N21, 118.7 (2); N1-Fe-N21, 81.3 (2); N1-Fe-O2, 84.7 (2); N11-Fe-N31, 153.3 (2).

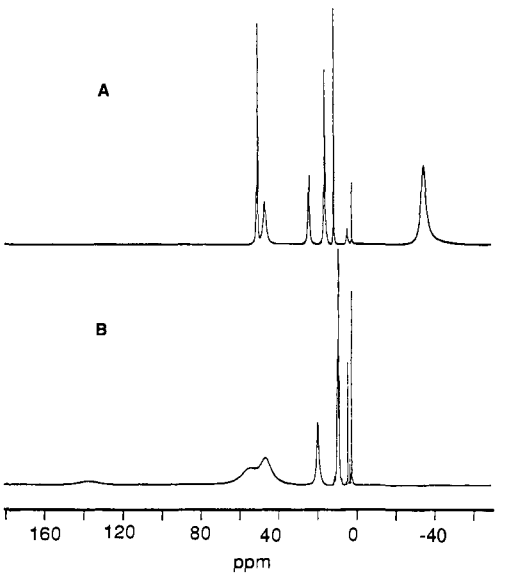

Figure 2. ^1H NMR spectra of **1** and **2** in CD_3CN. The peak assignments are deduced from peak integration and T_1 (ms) measurements. (A) $[Fe^{II}(TLA)(BF)](ClO_4)$ (**1**): BF *o*-H at 24 ppm (2.4 ms), *m*-H at 11 ppm (15 ms), and *p*-H at 16 ppm (~17 ms); TLA β-H at 50 ppm (7.3 ms) and 46 ppm (3.0 ms), γ-H at 16 ppm (~17 ms), α-CH_3 at -35 ppm (0.6 ms). (B) $[Fe^{II}(TPA)(BF)](ClO_4)$ (**2**): BF *o*-H at 9.0 ppm (4.5 ms), *m*-H at 8.6 ppm (32 ms), and *p*-H at 8.2 ppm (60 ms); TPA α-H at 137 ppm (1.1 ms), CH_2 at 53 ppm (2.4 ms), β-H at 46 ppm (8.4 ms), and γ-H at 20 ppm (22 ms).

(1) For reviews, see: (a) Abbott, M. T.; Udenfriend, S. *Molecular Mechanisms of Oxygen Activation*; Hayaishi, O., Ed.; Academic Press: New York, 1974; Chapter 5. (b) Hanauske-Abel, H. M.; Günzler, V. *J. Theor. Biol.* **1982**, *94*, 421-455. (c) Townsend, C. A.; Basak, A. *Tetrahedron* **1991**, *47*, 2591-2602.

(2) Hamilton, G. A. *Prog. Bioorg. Chem.* **1971**, *1*, 83-157.

(3) Lindblad, B.; Lindstedt, G.; Tofft, M.; Lindstedt, S. *J. Am. Chem. Soc.* **1969**, *91*, 4604-4606.

(4) (a) Myllylä, R.; Kaska, D. D.; Kivirikko, K. I. *Biochem. J.* **1989**, *263*, 609-611. (b) Majamaa, K.; Günzler, V.; Hanauske-Abel, H. M.; Myllylä, R.; Kivirikko, K. I. *J. Biol. Chem.* **1986**, *261*, 7819-7823. (c) Majamaa, K.; Hanauske-Abel, H. M.; Günzler, V.; Kivirikko, K. I. *Eur. J. Biochem.* **1984**, *138*, 239-245. (d) Nietfeld, J. J.; De Jong, L.; Kemp, A. *Biochim. Biophys. Acta* **1982**, *704*, 321-325. (e) Tuderman, L.; Myllylä, R.; Kivirikko, K. I. *Eur. J. Biochem.* **1977**, *80*, 341-348 and 349-357.

(5) (a) Bradley, F. C.; Lindstedt, C.; Lipscomb, J. D.; Que, L., Jr.; Roe, A. L.; Rundgren, M. *J. Biol. Chem.* **1986**, *261*, 11693-11696. (b) Pascal, R. A., Jr.; Oliver, M. A.; Chen, Y. C. J. *Biochemistry* **1985**, *24*, 3158-3165. (c) Lindblad, B.; Lindstedt, G.; Lindstedt, S. *J. Am. Chem. Soc.* **1970**, *92*, 7446-7449. (d) Fellman, J. H.; Fujita, T. S.; Roth, E. S. *Biochim. Biophys. Acta* **1972**, *284*, 90-100.

(6) (a) Thornburg, L. D.; Stubbe, J. *J. Am. Chem. Soc.* **1989**, *111*, 7632-7633. (b) Holme, E.; Lindstedt, G.; Lindstedt, S.; Tofft, M. *J. Biol. Chem.* **1971**, *246*, 3314-3319.

(7) (a) Günzler, V.; Majamaa, K.; Hanauske-Abel, H. M.; Kivirikko, K. I. *Biochim. Biophys. Acta* **1986**, *873*, 38-44. (b) De Jong, L.; Kemp, A. *Biochim. Biophys. Acta* **1982**, *709*, 142-145.

(8) (a) Lindstedt, S.; Rundgren, M. *J. Biol. Chem.* **1982**, *257*, 11922-11931. (b) Denum, J.; Lindstedt, S.; Rundgren, M. *Oxidases Relat. Syst., Proc. Int. Symp., 3rd* **1982**, 519-542.

(9) Holme, E.; Lindstedt, S. *Biochim. Biophys. Acta* **1982**, *704*, 278-283.

(10) (a) Counts, D. F.; Cardinale, G. J.; Udenfriend, S. *Proc. Natl. Acad. Sci. U.S.A.* **1978**, *75*, 2145-2149. (b) Roe, N. V.; Adams, E. *J. Biol. Chem.* **1978**, *253*, 6327-6330. (c) Holme, E.; Lindstedt, S.; Nordin, I. *Biochem. Biophys. Res. Commun.* **1982**, *107*, 518-524. (d) Holme, E.; Lindstedt, S.; Nordin, I. *Biosci. Rep.* **1984**, *4*, 433-440. (e) Holme, E.; Lindstedt, G.; Lindstedt, S. *Acta Chem. Scand. Ser. B* **1979**, *33*, 621-622.

(11) De Mota, M. M.; Rodgers, J.; Nelson, S. M. *J. Chem. Soc. A* **1969**, 2036-2044.

(12) Gafford, B. G.; Holwerda, R. A. *Inorg. Chem.* **1989**, *28*, 60-66.

(13) Abbreviations used: BF, benzoylformate; OAc, acetate; OBz, benzoate; TPA, tris(2-pyridylmethyl)amine; TLA, tris[(6-methyl-2-pyridyl)-methyl]amine.

0002-7863/92/1514-7567$03.00/0